Electronic supplementary information for:

Charge Transfer from Perovskite Oxide Nanosheet to N-doped Carbon Nanotube to Promote Enhanced Performance of Zinc-air Battery

*Rahul Majee, Surajit Mondal and Sayan Bhattacharyya**

Department of Chemical Sciences, and Centre for Advanced Functional Materials, Indian Institute of Science Education and Research (IISER) Kolkata, Mohanpur - 741246, India

*Email for correspondence: sayanb@iiserkol.ac.in

Experimental Section

Materials

Praseodymium nitrate [$Pr(NO_3)_3$, Alfa Aesar, 99%], barium nitrate [$Ba(NO_3)_2$, Alfa Aesar, 99%], cobalt nitrate hexahydrate [$Co(NO_3)_2.6H_2O$, Merck, 99%], manganese acetate tetrahydrate [$Mn(CH_3COO)_2.6H_2O$, Merck, 99%], glycine (Merck, 99%), multiwalled carbon nanotube (CNT, Technistro, >99%), urea (Merck, 98%) were used without further purification. Distilled water was used during synthesis and electrochemical tests unless specified. Potassium hydroxide (KOH, Merck, 98%) was used to prepare the electrolyte.

Synthesis of $BaPrMn_{1.75}Co_{0.25}O5_{+\delta}$ nanosheet (BPMC NS)

For the synthesis of BPMC NSs, Ba-, Pr-, Co-nitrate salts and Mn-acetate in 1:1:0.25:1.75 molar ratio were mixed and dissolved in distilled water. The pH of this clear solution was adjusted to 6.5 by adding dilute ammonia followed by the addition of glycine under stirring. The molar ratio of metal precursors and glycine was kept at 1:1. The solution was heated at 80°C to evaporate the solvent forming the BPMC gel. The gel was further heated to obtain a gray powder which was dried at 150°C for 2h. The dried powder was calcined at 950°C for 5 h in the air followed by reduction at 750°C for 5 h in 5% H_2 in Ar to obtain the pure phase of BPMC NS.

Synthesis of NCNT

Weighed amounts of CNTs were refluxed overnight in 1:1 HNO_3:H_2SO_4 mixture, the residue collected after washing with distilled water several times and dried in a hot air oven at 60°C. Thereafter a mixture of treated CNT and urea in 1:3 weight ratios was transferred to teflon sealed autoclave for the hydrothermal reaction at 150°C for 12h to obtain the NCNTs.

Synthesis of BPMC/NCNT

A weighed amount of BPMC NSs was dispersed in ethanol and magnetically stirred to produce a fine dispersion of the low dimensional NSs. Calculated amounts of the as prepared NCNTs viz. 5, 10 and 20 wt% were also dispersed in ethanol by probe sonication. Each of the weighed NCNT dispersions was separately added to the finely dispersed BPMC NSs in ethanol under constant stirring overnight. BPMC/NCNT composites were collected by centrifugation at 6000 rpm which were finally dried in a hot air oven for further use. The spatial connectivity between the components was achieved through strong electrostatic interaction.

Physicochemical characterization

Powder X-ray diffraction (PXRD) patterns were recorded with Rigaku Smart Lab (mini flex II) Powder X-ray diffractometer. Cu Kα (λ=1.5403 Å) was used with Bragg Brentano filter for diffraction. Scan rate was maintained at $2\theta = 1^{\circ}$/min for the data used for Rietveld refinement by GSAS-II software. The zeta potential was measured by Malvern Zetasizer Nano ZS equipped with 4.0 mW HeNe laser operating at λ = 633 nm. Transmission electron microscopy (TEM) analyses were performed in JEOL 2100F electron microscope (IISER Kolkata DST-FIST facility) at an operating acceleration voltage 200 kV and corresponding elemental maps were obtained using Oxford X-max solid state Si drift X-ray detector. The NS thickness measurement was performed by atomic force microscopy (AFM) using Nova NT-MDT instrument with the samples drop casted on clean Si substrate. Elemental abundances were calculated by energy dispersive X-ray spectroscopy (EDS) collected in Carl Zeiss SUPRA 55VP FESEM instrument with Oxford EDS analyzer. The amount of nitrogen in NCNT was estimated by CHN elemental analyzer. Raman spectrum was recorded with 633 nm line of a He-Ne ion laser as the excitation source (LABRAM HR800) Horiba Raman spectrophotometer. FTIR spectroscopy was carried out in a Perkin Elmer spectrum RX1 instrument.

Electrochemical characterization

The electrodes were prepared by drop-casting as prepared catalyst ink (5 mg of catalyst and 10 μL Nafion in 0.49 mL of isopropanol). For OER 10 μL was drop casted onto PTFE treated carbon fiber paper (Toray, thickness 0.25 μm) with an approximate geometrical area of 0.25 cm^2. The catalyst loading of 0.4 $mg \cdot cm^{-2}$ was kept the same for ORR measurements, where 2 μL catalyst ink was drop casted onto a glassy carbon RDE over 0.125 cm^2 area and allowed to dry. 1M KOH was taken as the electrolyte and all electrochemical measurements were performed in a Biologic potentiostat (VSP-300), where Ag/AgCl (3 M KCl) and Pt wire were used as reference and counter electrode, respectively. To obtain stable electrochemical interface, 40 cyclic voltammogram (CV) cycles were performed before collecting the data. Uncompensated solution resistance (*iR*) was adjusted in the final reported data. The scan range 1.2 to 2 V and 1 to 0.2 V versus RHE at sweep rate of 10 $mV \cdot s^{-1}$ were kept to collect the OER and ORR linear sweep voltammograms (LSV), respectively. ORR experiments were done in O_2 saturated electrolyte and the LSV polarization plots were taken at 1600 rpm rotation speeds of RDE. Tafel plots were obtained by plotting overpotential with respect to the logarithm of the corresponding current densities (log j). Electrochemical impedance spectroscopy (EIS) measurements were carried out at a bias potential of 1.68 and 0.8 V versus RHE for OER and ORR, respectively. The trend in ECSA was observed from the double layer capacitance (C_{dl}) values that were determined from CV measurements in the non-faradic region, -0.05 to 0.05 V, at different scan rates from 10 to 60 mV/s. The chronopotentiometric stability tests (CP) were performed at 10 and -1 mA/cm^2 current density for OER and ORR, respectively. The number of electron transfer (n) and percent H_2O_2 formation in ORR were estimated following equations S1 and S2.

$$n = \frac{I_{disk}}{I_{disk} + \frac{I_{ring}}{N_c}} \quad \text{(S1)}$$

$$\%H_2O_2 = \frac{2\frac{I_{ring}}{N_c}}{I_{disk} + \frac{I_{ring}}{N_c}} 100\% \quad \text{(S2)}$$

where I_{disk} is the disk current, I_{ring} is the ring current, and N_{c} is the collection efficiency (42.7%). Mott-Schottky experiments were performed after drop casting BPMC/NCNT samples dispersed in isopropanol onto polished glassy carbon electrode. Analysis was performed in the frequency range 1 MHz to 100 Hz using alternating current in the DC bias range from -2 to +2 V versus Ag/AgCl. Flat band potential (E_{fb}) was calculated from Mott-Schottky plot (using equation S3).[S1]

$$\frac{1}{C_s^2} = \frac{2}{\varepsilon\, \varepsilon_0 A^2 e N_d}\left(E - E_{fb} - \frac{k_B T}{e}\right) \quad \text{(S3)}$$

where C_s is the differential capacitance $\partial Q/\partial E$, ε and ε_0 are the dielectric constants of the semiconductor (specific to the electrode) and the permittivity of free space (8.85×10^{-12} F/m), respectively, A is the area, e is the elementary charge (1.6×10^{-19} C), N_d is the density of dopants (specific to the electrode), E is the applied potential (specific to the electrode), E_{fb} is the flat band potential (specific to the electrode), k_B is Boltzmann constant (1.38×10^{-23} J/K) and T is the absolute temperature (298 K).

Rechargeable Zn-air battery (ZAB) tests

All battery characterizations were carried out in a homemade teflon cased ZAB consisting of polished Zn plate (Alfa Aesar, thickness = 0.25 mm) as the anode and catalyst drop casted on carbon cloth gas diffusion layer (1 mg/cm^2) as the gas diffusion electrode. The electrolyte used was 0.2 M zinc acetate solution in 6 M KOH. Charge discharge polarization plots were obtained by LSV with 5 mV/s scan rate. Galvanostatic charge/discharge profiles were obtained at 5 mA/cm^2 in an ambient atmosphere. Charge discharge cycling was done at a current density of 5 mA/cm^2 with 1h cycle duration.

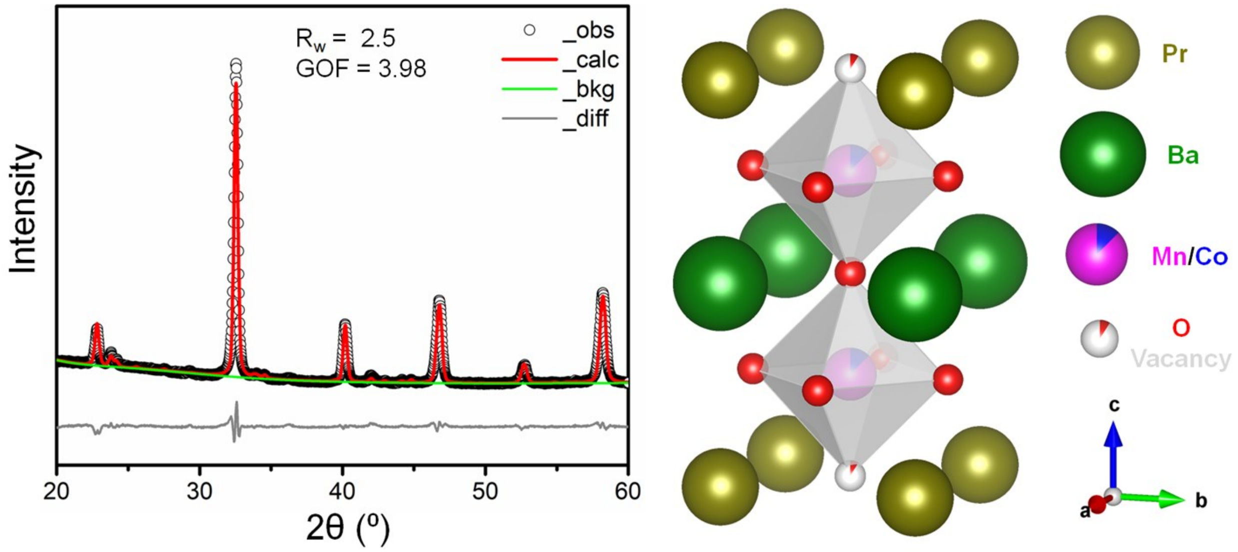

Fig. S1 Rietveld analysis of PXRD pattern of BPMC and corresponding schematic of the unit cell.

Table S1 PXRD Rietveld refinement parameters of BPMC NSs.

Major Phases	Space group	Volume (Å^3)	Lattice parameter (Å)		δ	GOF	R_w
			a	*C*			
$BaPrMn_{1.75}Co_{0.25}O_{5+\delta}$	*P4/mmm*	116.38	3.8703	7.7691	0.09	3.98	2.5

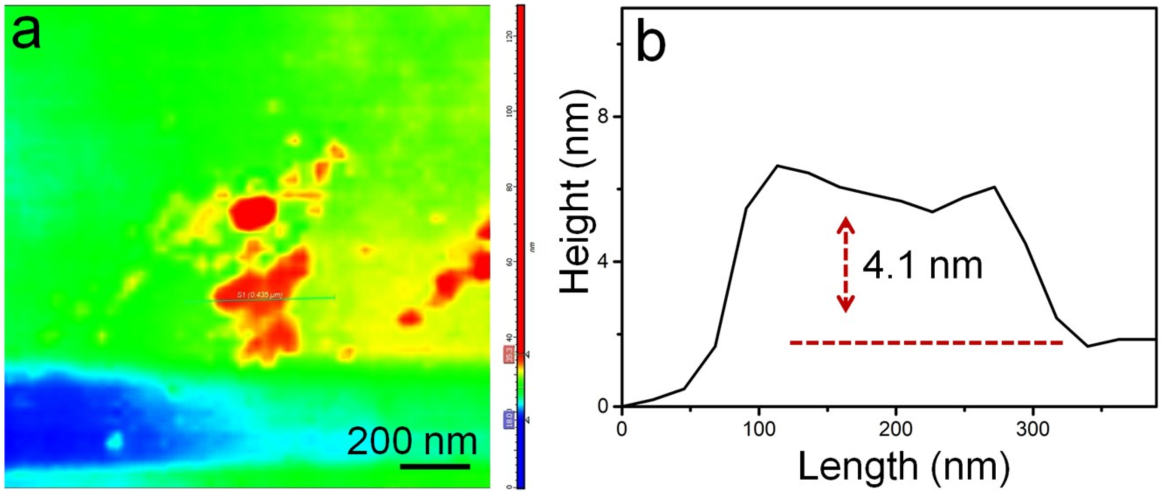

Fig. S2 (a) AFM image of BPMC NSs and (b) corresponding height profile.

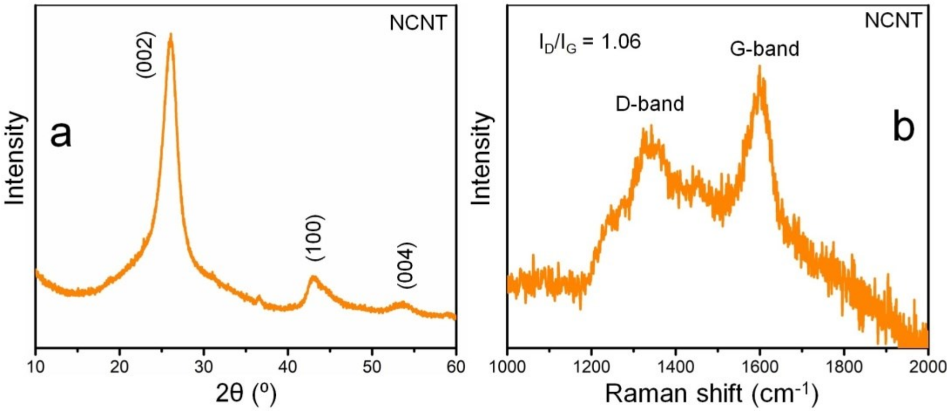

Fig. S3 (a) PXRD pattern and (b) Raman spectrum of NCNT.

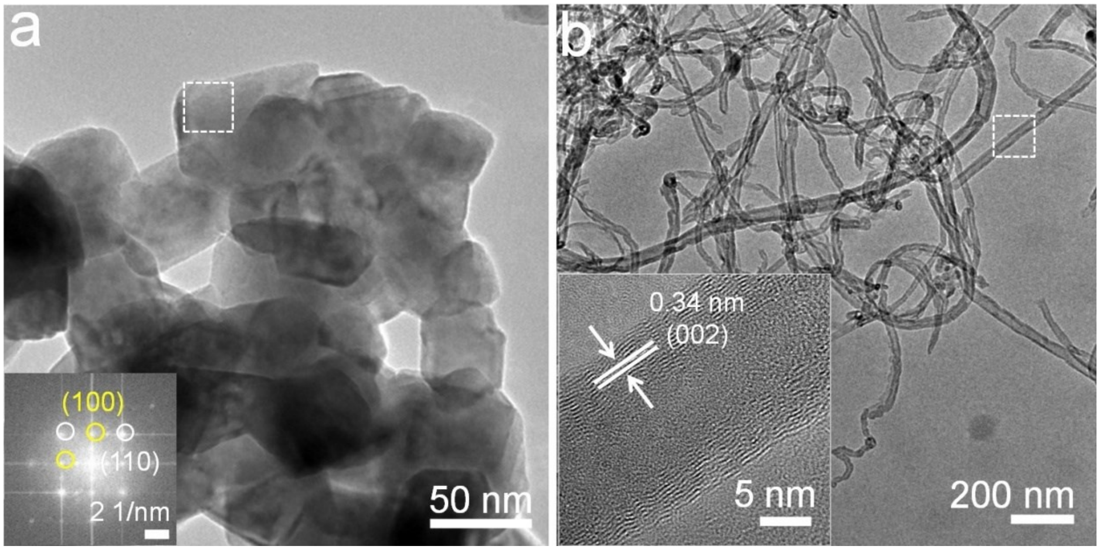

Fig. S4 TEM image of (a) BPMC NSs and (b) NCNT. Inset (a) shows the FFT pattern from the region marked with dotted box. Inset (b) shows the HRTEM image of NCNT.

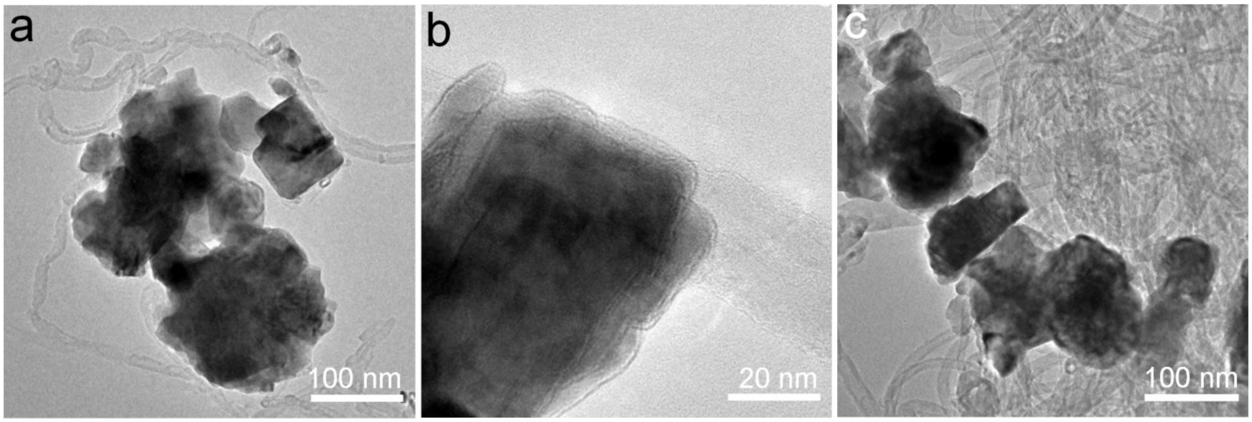

Fig. S5 TEM images of (a) BPMC/NCNT-5, (b) BPMC/NCNT-10 and (c) BPMC/NCNT-20.

Table S2 EDS analysis of BPMC/NCNT samples obtained from scanning electron microscope.

Sample	Element (at%)						
	Ba	Pr	Mn	Co	O	C	N
BPMC	10.8 ±1	11.3 ± 1.8	13.2±3.2	3.1±0.9	61.6±4.3	0	0
BPMC/NCNT-5	8.4±0.7	8.3±1.2	11.9±2.7	2.6±0.2	64.5±3	36.5±5.1	2.0±0.6
BPMC/NCNT-10	4.8±1.9	6.7±1.1	8.5±1.6	0.9±0.5	38.2±1.7	39.6±2	1.3±0.9
BPMC/NCNT-20	3.7±1.08	3.6±0.6	5.3±1.4	1.1±0.7	28.8±1.0	55±4.8	2.5±0.3

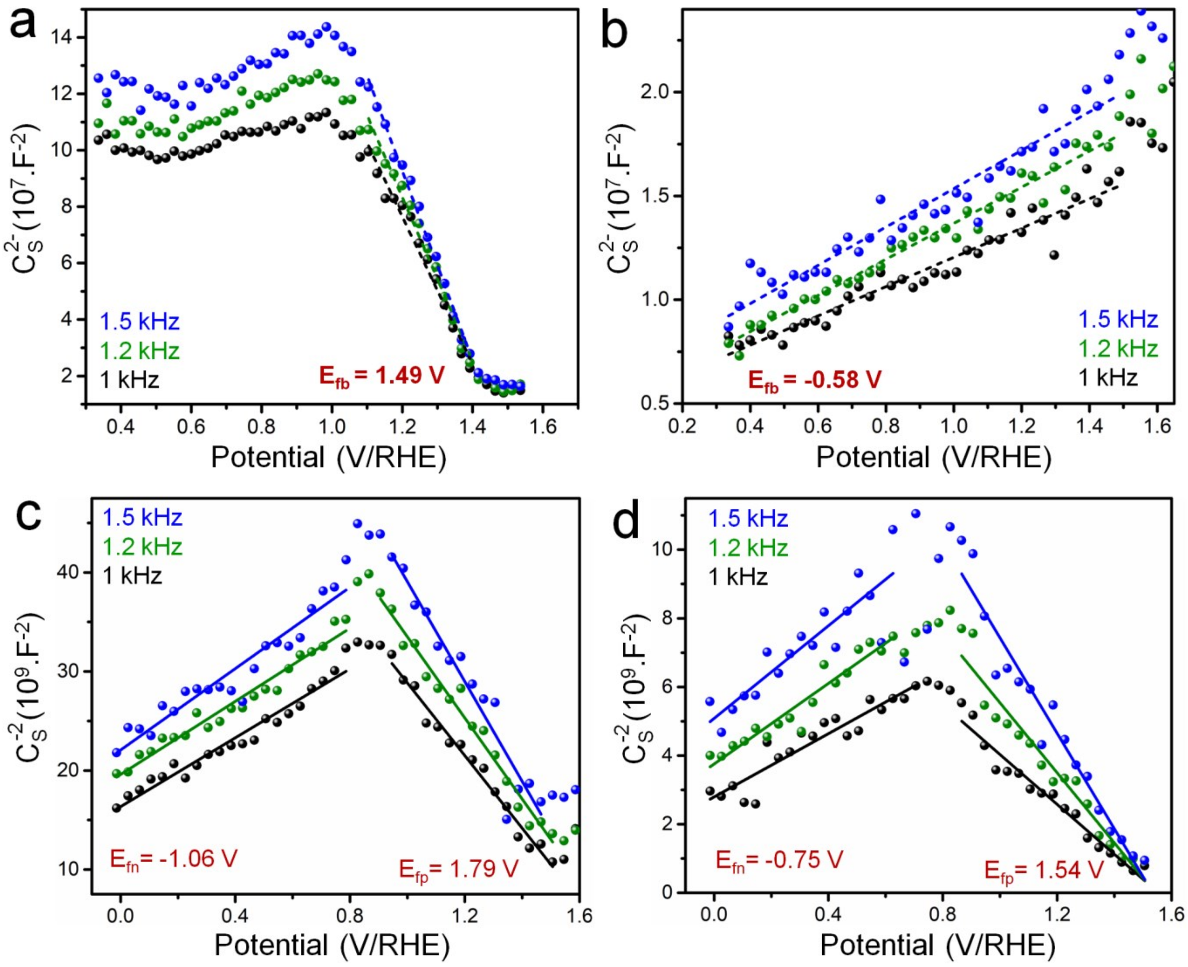

Fig. S6 Mott-Schottky plots of (a) BPMC, (b) NCNT, (c) BPMC/NCNT-5 and (d) BPMC/NCNT-20.

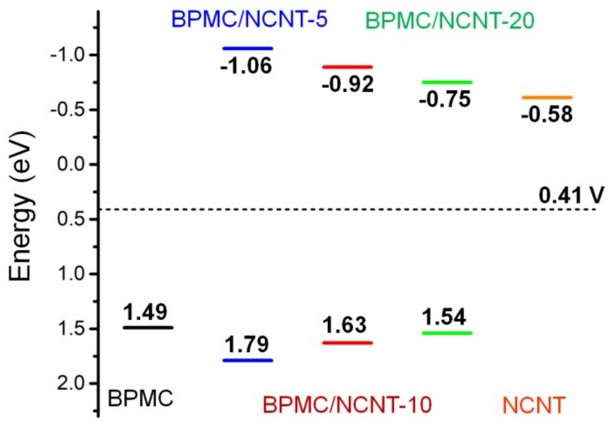

Fig. S7 Flat band energy profile of different BPMC and NCNT composites obtained from Mott-Schottky plots. 0.41 V is the thermodynamic potential for oxygen electrolysis in alkaline electrolyte.

Calculation of carrier density

The carrier density (N_d) is calculated from the slope of Mott Schottky plot by equation (S4):

$$Slope = \frac{2}{\varepsilon\varepsilon_0 A^2 N_d e} \qquad \text{(S4)}$$

where ε is dielectric constant of the material, ε_0 is permittivity of free space (8.85×10^{-7} mF/m), A is area of the electrode (0.125 cm^2) and e is the elementary charge (1.6×10^{-19} C).

Table S3 Parameters obtained from carrier density calculations.

C_{dl} is the double layer capacitance of the electrode, calculated from CV plots at different scan rates (see Fig. S11), $C_0 = \varepsilon_0.A/t$; where t is the thickness of the film (~25 nm, from AFM study). The negative charge carrier (electron) density of BPMC/NCNT-10 is an order of magnitude higher than the other composites endowing its finer ORR activity. BPMC/NCNT-20 having a moderately higher hole density and lower electron density makes it a fitter OER catalyst.

Catalyst	C_{dl} (mF)	ε (= C_{dl}/C_0)	Slope (*p*-type)	Slope (*n*-type)	N_d (hole)	N_d (electron)
BPMC	0.1	226	2.9	-	1.34×10^{25}	-
BPMC/NCNT-5	0.67	1514	0.041	0.0185	1.41×10^{26}	3.14×10^{26}
BPMC/NCNT-10	1.43	3232	0.0038	0.0025	7.16×10^{26}	1.09×10^{27}
BPMC/NCNT-20	1.94	4384	0.0102	0.0059	1.97×10^{26}	3.4×10^{26}
NCNT	1.42	3209	-	0.0093	-	2.94×10^{26}

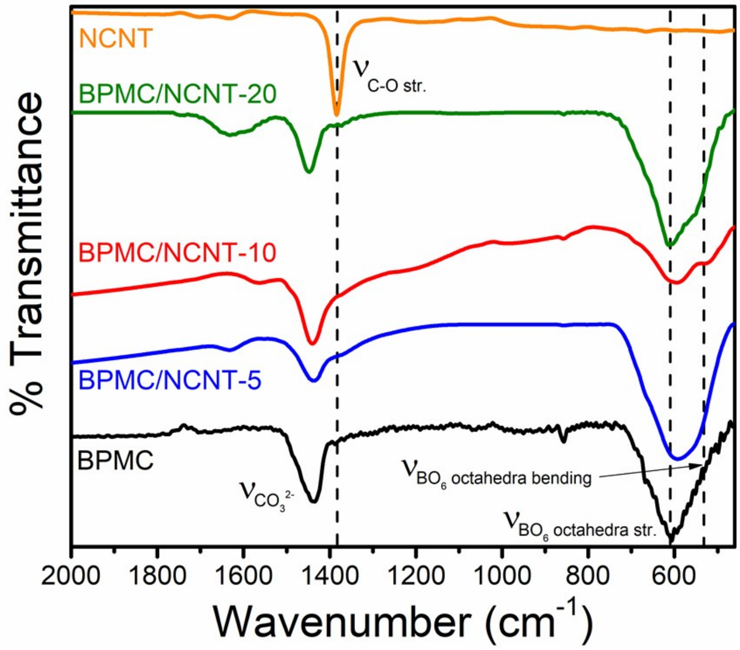

Fig. S8 Fourier-transform infrared (FTIR) spectra of BPMC, BPMC/NCNT-5/10/20 and NCNT.

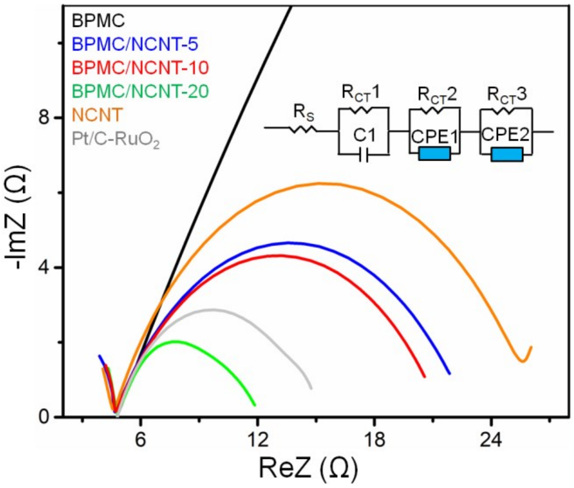

Fig. S9 Nyquist plots at 1.68 V (RHE) for BPMC, NCNT, BPMC/NCNT composites and Pt/C-RuO$_2$.

Table S4 List of parameters obtained from the fitting of Nyquist plots. R_s is solution resistance (Ω), R_{CT} is charge transfer resistance (Ω), C is the capacitor (F), CPE is constant phase element ($F.s^{a-1}$), where a is the CPE-exponent related to frequency dispersion between 0 to 1.

Catalyst	R_s (Ω)	$R_{CT}1$ (Ω)	$R_{CT}2$ (Ω)	$R_{CT}3$ (Ω)	$C1$ (F)	$CPE1$ ($F.s^{a-1}$)	$CPE2$ ($F.s^{a-1}$)
OER							
BPMC	3.8	8.9	5.4	130.3	1×10^{-3}	7×10^{-2} ($a = 1$)	9×10^{-4} ($a = 0.6$)
BPMC/NCNT-5	1.9	3.0	2.9	14.2	9×10^{-2}	6.7×10^{-7} ($a = 0.8$)	2.9×10^{-3} ($a = 0.67$)
BPMC/NCNT-10	0.4	5.5	6.4	3.8	1.1×10^{-8}	1.6×10^{-3} ($a = 0.87$)	1×10^{-1} ($a = 0.31$)
BPMC/NCNT-20	0.9	1.6	5.8	12.7	2.4×10^{-3}	1.5×10^{-2} ($a = 0.56$)	1.1×10^{-9} ($a = 0.87$)
NCNT	0.3	8.8	21.6	34.8	1.4	2.1×10^{-3} ($a = 0.67$)	5.8×10^{-9} ($a = 0.78$)
ORR							
BPMC	3.7	101.8	1412	1197	8.1×10^{-4}	7.2×10^{-5} ($a = 0.66$)	2.1×10^{-3} ($a = 0.45$)
BPMC/NCNT-5	17.1	66.9	129	2659	2.4×10^{-9}	4.1×10^{-4} ($a = 0.61$)	3.7×10^{-6} ($a = 0.99$)
BPMC/NCNT-10	4.7	311.5	818.6	18.8	9×10^{-3}	2.2×10^{-6} ($a = 0.59$)	1.7×10^{-9} ($a = 0.94$)
BPMC/NCNT-20	20.1	92.8	210.2	1427	6×10^{-1}	2.2×10^{-5} ($a = 0.98$)	5.2×10^{-4} ($a = 0.57$)
NCNT	19.4	39	774.5	2616	3.9×10^{-5}	1.4×10^{-3} ($a = 1$)	1.7×10^{-4} ($a = 0.72$)

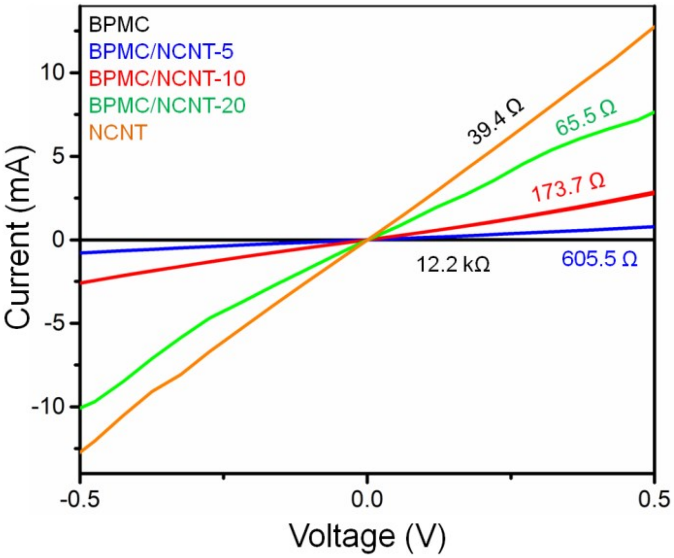

Fig. S10 Current-voltage plots of BPMC, NCNT and BPMC/NCNT composites.

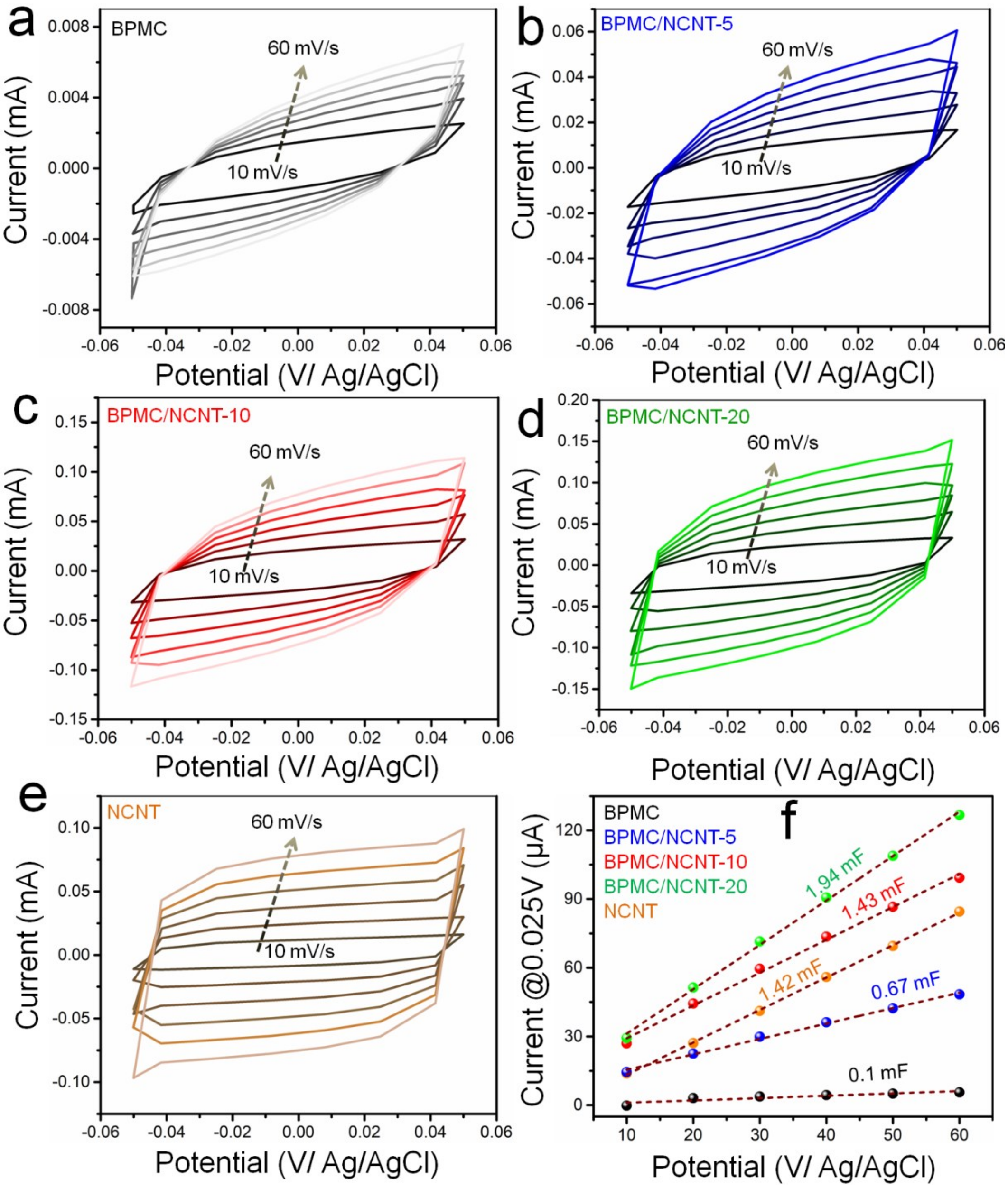

Fig. S11 (a-e) Cyclic voltammograms at different scan rates to determine C_{dl} of different BPMC/NCNT samples. (f) Current-scan rate plots where the slope of the fitted line gives C_{dl}.

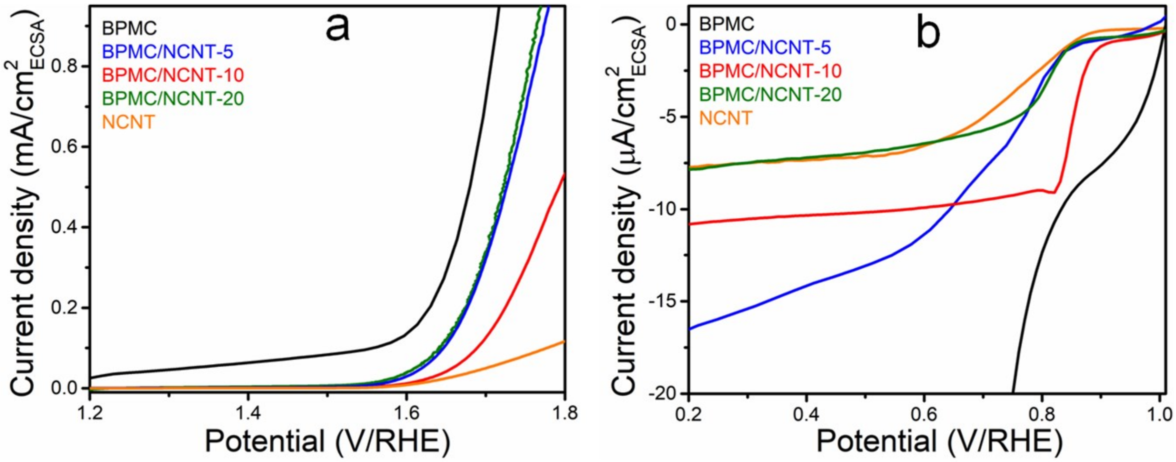

Fig. S12 Electrochemically active surface area (ECSA) normalized activity towards (a) OER and (b) ORR.

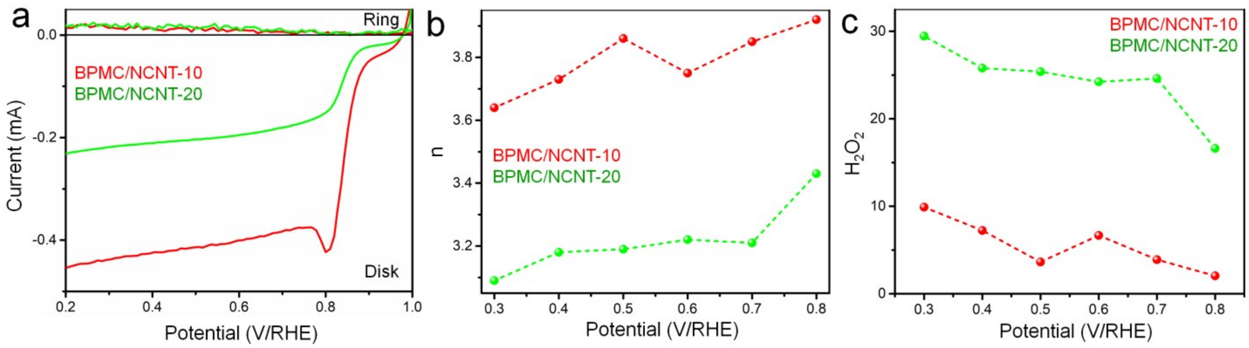

Fig. S13 RRDE experiments at 1600 rpm to measure the number of electron transfer (*n*) and percent of H_2O_2 formation for BPMC/NCNT-10 and BPMC/NCNT-20. (a) Ring and disk current in the ORR range. Plots of (b) *n* and (c) H_2O_2 yield at different potentials.

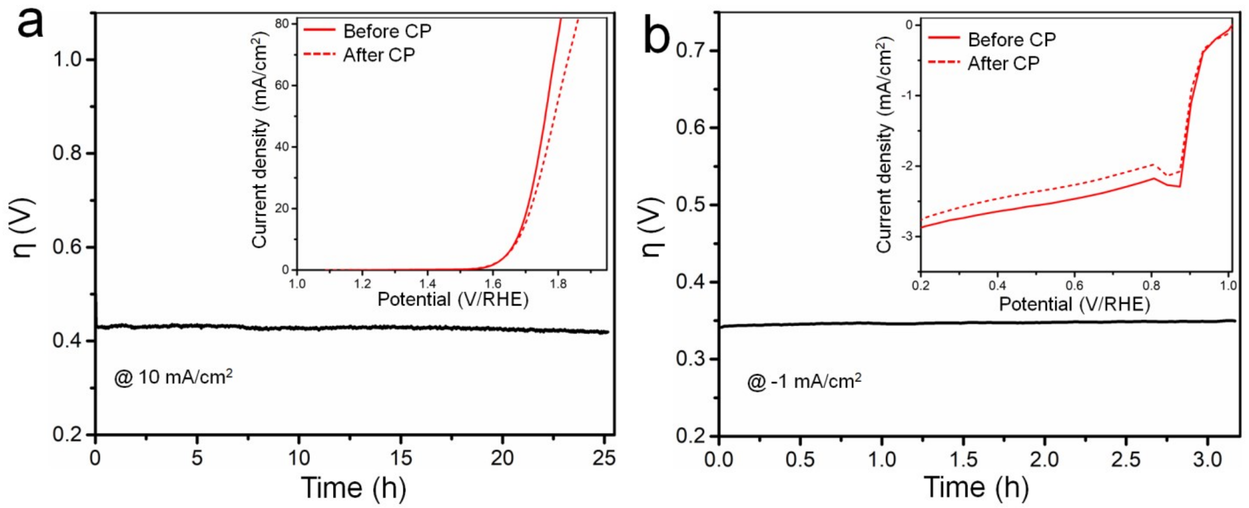

Fig. S14 Chronopotentiometric stability test of BPMC/NCNT-10 electrode for (a) OER and (b) ORR. Insets show the LSV plots before and after the stability tests.

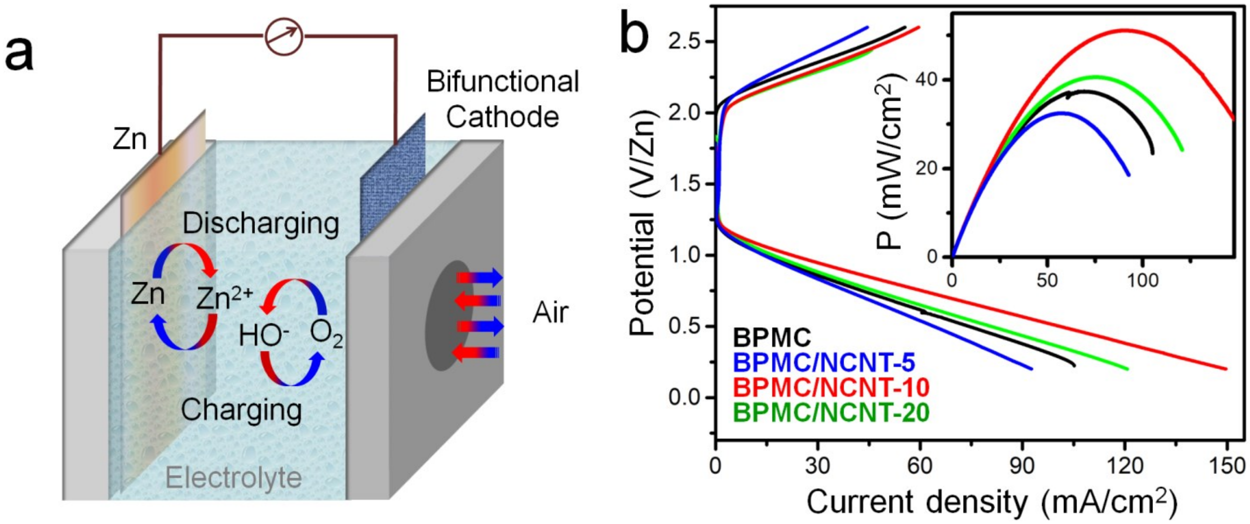

Fig. S15 Rechargeable ZAB performance: (a) Schematic diagram of homemade ZAB and charge/discharge cycles. (b) Polarization plots with different BPMC cathode materials.

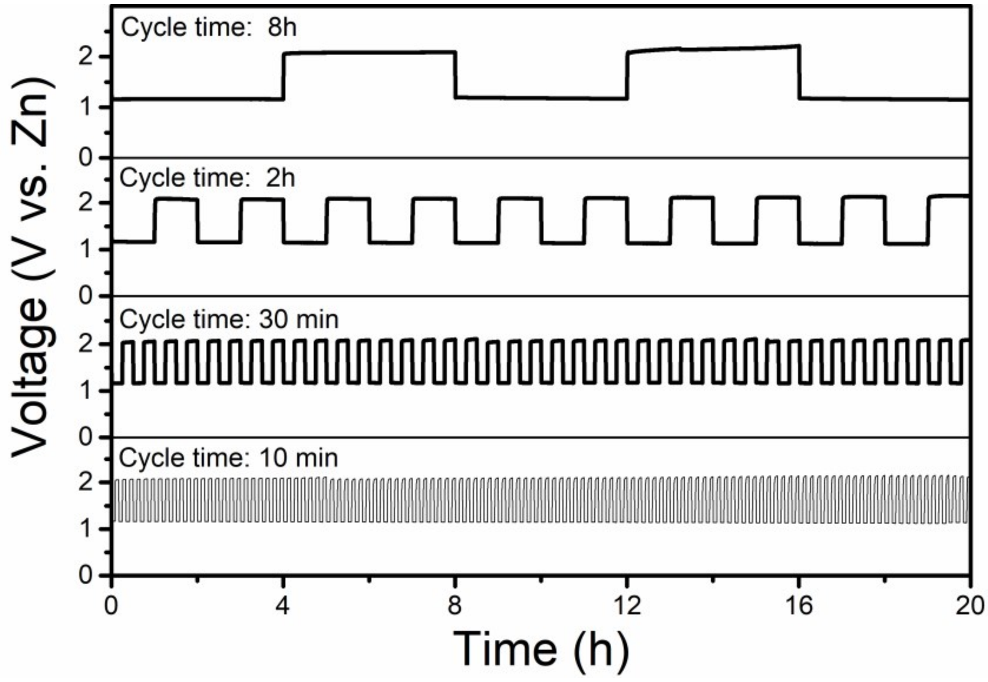

Fig. S16 Galvanostatic cyclic tests of rechargeable Zn-air battery with BPMC/NCNT-10 cathode at 5 mA/cm^2 for 20h with different cycle times. No significant alteration in the voltage gap between discharge and charge is observed.

Table S5 Literature comparison of Zn-air battery parameters for BPMC/NCNT-10 cathode with recently reported perovskite oxide-carbon composite cathodes.

Supplementary References

S1 K. Gelderman, L. Lee and S. W. Donne, *J. Chem. Educ.*, 2007, **84**, 685–688.

Sr. No	Material	Fabrication conditions & The role of C composite	Specific capacity; Cyclic stability (time per cycle)	Ref.
1	$(\alpha\text{-}MnO_2)_2\text{-}(LaNiO_3)_3]_{40\%}/(CNT)_{60\%}$	Ex-situ assembling of $LaNiO_3$ ($900^{o}C$), MnO_2 and CNT by sonication at $60^{o}C$. To improve the electronic conductivity.	75 cycle @30 $mA.cm^{-2}$ (10 min)	S2
2	$LaTi_{0.65}Fe_{0.35}O_{3-\delta}$ on N doped C nanorod	Carbon source added to electrospinning precursor and calcination at $800^{o}C$. Synergistic catalysis.	789.2 $mA.h/g_{Zn}$, 6 h @5 A/g (1h)	S3
3	$LaMn_{0.9}Co_{0.1}O_3$ /NCNT	At first perovskite synthesized at $850^{o}C$ then grown carbon at $700^{o}C$. To enhance the surface area for utilization.	66 cycle @18 $mA.cm^{-2}$	S4
4	$LaNiO_3$/NCNT	As prepared $LaNiO_3$ ($800^{o}C$) with ferrocene and ethylenediamine to grow NCNT at $700^{o}C$ To improve the diffusion of reactants and charge transfer through inter-particle interaction.	10 cycle @17.6 $mA.cm^{-2}$ (4h)	S5
5	$La_{0.99}MnO_{3.03}$ /30wt% C	Vulcan carbon added to precursor gel then heated at $180^{o}C$ in presence of KOH, then treated with HNO_3 to obtain the final product. Reduced particle size, high surface area, homogenous distribution, strong oxide-carbon coupling and improved conductive network formation.	670 $mA.h/g_{Zn}$, @10 mA/cm^2 Non-rechargeable	S6
6	$La_{0.6}Ca_{0.4}CoO_3$ /50wt% graphitic carbon	The perovskite was made at $800^{o}C$. Physical mixing in the catalysts ink by sonication.	750 $mA.h/g_{Zn}$, >1000 cycle @50 $mA.cm^{-2}$ (10 min)	S7
7	$LaMn_{0.9}Co_{0.1}O_3$-graphene	Metal precursors added to the graphene solution and blended followed by calcination at $600^{o}C$. To improve conductivity and porosity.	OCV of 1.165 V @20 mA/cm^2	S8
8	$LaNiO_3$ nanorods/ RGO	Metal precursor added to RGO dispersion then hydrothermal treatment at $180^{o}C$ followed by calcination at $650^{o}C$. To enhance the active site of $LaNiO_3$.	97 cycle @25 $mA.cm^{-2}$ (1h)	S9
9	$La_{0.6}Sr_{0.4}Fe_{0.8}Co_{0.2}O_3$/ carbon black	Perovskite obtained at $800^{o}C$ mixed with commercial carbon followed by ball milling for 2h. To enhance active sites and electrical conductivity.	21 cycle @80 $mA.cm^{-2}$ (4min)	S10
10	$(PrBa_{0.5}Sr_{0.5})_{0.95}Co_{1.5}Fe_{0.5}O_{5+\delta}$ 3D N-doped graphene	Electrospinning followed by calcination ($700^{o}C$) Synergistic catalytic activity; N-doped graphene provides the ORR activity	18.3h @10$mA.cm^{-1}$ (10min)	S11
11	Pt-$Sr(Co_{0.8}Fe_{0.2})_{0.95}P_{0.05}O_{3-\delta}$/C	Ball milling of calcined ($1100^{o}C$) product with Super P Carbon which is a conducting agent and influences the ORR activity	790.4 $mA.h/g_{Zn}$, 80h @5$mA.cm^{-2}$ (1h)	S12
12	$NdBa_{0.5}Sr_{0.5}Co_{1.5}Fe_{0.5}O_{5+\delta}$ + N-CNT + cellulose nanofiber	The physical mixture obtained by freeze-drying @-$12^{o}C$ of perovskite ($900^{o}C$) with commercial N-CNT. Synergistic catalytic improvement	Flexible battery 15h@1$mA.cm^{-2}$ (10min)	S13
13	BPMC/NCNT-10	Room temp through electrostatic interaction. Synergistic effect and experimental found charge transfer between BPMC and NCNT	789.2 $mA.h/g_{Zn}$ (20.1h); >85h @ 5 $mA.cm^{-2}$ (1h)	This work

S2 H. Ma and B. Wang, *RSC Adv.*, 2014, **4**, 46084–46092.
S3 M. Prabu, P. Ramakrishnan, P. Ganesan, A. Manthiram and S. Shanmugam, *Nano Energy*, 2015, **15**, 92–103.
S4 D. U. Lee, M. G. Park, H. W. Park, M. H. Seo, V. Ismayilov, R. Ahmed and Z. Chen, *Electrochem. commun.*, 2015, **60**, 38–41.
S5 D. U. Lee, H. W. Park, M. G. Park, V. Ismayilov and Z. Chen, *ACS Appl. Mater. Interfaces*, 2015, **7**, 902–910.
S6 Z. Yan, H. Sun, X. Chen, X. Fu, C. Chen, F. Cheng and J. Chen, *Nano Res.*, 2018, **11**, 3282–3293.
S7 T. Ishihara, L. M. Guo, T. Miyano, Y. Inoishi, K. Kaneko and S. Ida, *J. Mater. Chem. A*, 2018, **6**, 7686–7692.
S8 J. Hu, L. Wang, L. Shi and H. Huang, *Electrochim. Acta*, 2015, **161**, 115–123.
S9 J. Hu, Q. Liu, Z. Shi, L. Zhang and H. Huang, *RSC Adv.*, 2016, **6**, 86386–86394.
S10 C. Alegre, E. Modica, A. S. Aricò and V. Baglio, *J. Electroanal. Chem.*, 2018, **808**, 412–419.
S11 Y. Bu, H. Jang, O. Gwon, S. Kim, S. Joo, G. Nam, S. Kim, Y. Qin, Q. Zhong, S. Kwak, J. Cho and G. Kim, *J. Mater. Chem. A*, 2019, **7**, 2048–2054.
S12 X. Wang, J. Sunarso, Q. Lu, Z. Zhou, J. Dai, D. Guan, W. Zhou and Z. Shao, *Adv. Energy Mater.* 2020, **10**, 1903271.
S13 D. Lee, H. Lee, O. Gwon, O. Kwon, H. Y. Jeong, G. Kim and S. Lee*, J. Mater. Chem. A*, 2019, **7**, 24231-24238.